

WASP-19b: the shortest period transiting exoplanet yet discovered

L. Hebb¹, A. Collier-Cameron¹, A.H.M.J. Triaud², T.A. Lister³, B. Smalley⁴, P.F.L. Maxted⁴,
C. Hellier⁴, D.R. Anderson⁴, D. Pollacco⁵, M.Gillon^{2,6}, D. Queloz², R.G. West⁷, S.Bentley⁴,
B. Enoch¹, C.A. Haswell⁸, K. Horne¹, M. Mayor², F. Pepe², D. Segransan², I. Skillen⁹, S. Udry²,

and

P.J. Wheatley¹⁰

ABSTRACT

We report on the discovery of a new extremely short period transiting extra-solar planet, WASP-19b. The planet has mass, $M_{\text{pl}} = 1.15 \pm 0.08 M_J$, radius, $R_{\text{pl}} = 1.31 \pm 0.06 R_J$, and orbital period, $P = 0.7888399 \pm 0.0000008$ days. Through spectroscopic analysis, we determine the host star to be a slightly super-solar metallicity ($[M/H] = 0.1 \pm 0.1$ dex) G-dwarf with $T_{\text{eff}} = 5500 \pm 100$ K. In addition, we detect periodic, sinusoidal flux variations in the light curve which are used to derive a rotation period for the star of $P_{\text{rot}} = 10.5 \pm 0.2$ days. The relatively short stellar rotation period suggests that either WASP-19 is somewhat young (~ 600 Myr old) or tidal interactions between the two bodies have caused the planet to spiral inward over its lifetime resulting in the spin-up of the star. Due to the detection of the rotation period, this system has the potential to place strong constraints on the stellar tidal quality factor, Q'_s , if a more precise age is determined.

Subject headings: stars: planetary systems – techniques: radial velocities – techniques: photometric

¹School of Physics and Astronomy, University of St Andrews, North Haugh, St Andrews, Fife KY16 9SS, UK

²Observatoire de Genève, Université de Genève, 51 Ch. des Maillettes, 1290 Sauverny, Switzerland

³Las Cumbres Observatory, 6740 Cortona Dr. Suite 102, Santa Barbara, CA 93117, USA

⁴Astrophysics Group, Keele University, Staffordshire, ST5 5BG, UK

⁵Astrophysics Research Centre, School of Mathematics & Physics, Queen's University, University Road, Belfast, BT7 1NN, UK

⁶Institut d'Astrophysique et de Gophysique, Université de Liège, Alle du 6 Aot, 17, Bat. B5C, Liège 1, Belgium

⁷Department of Physics and Astronomy, University of Leicester, Leicester, LE1 7RH, UK

⁸Department of Physics and Astronomy, The Open University, Milton Keynes, MK7 6AA, UK

⁹Isaac Newton Group of Telescopes, Apartado de Correos 321, E-38700 Santa Cruz de la Palma, Tenerife, Spain

¹⁰Department of Physics, University of Warwick, Coventry CV4 7AL, UK

1. Introduction

Since the unexpected discovery of the first ‘hot Jupiter’, 51 Peg b (Mayor & Queloz 1995), exoplanets with an exceptionally wide variety of properties have been detected which have dramatically changed our understanding of planetary physics. In particular, through the discovery of various transiting planets, we have learned that extra-solar planets can have radii much larger than Jupiter (e.g. Hebb et al. 2009) or densities much higher (Sato et al. 2005). Many, but not all, ‘hot Jupiters’ have temperature inversions in their atmospheres (e.g. Knutson et al. 2008), and they can have very low optical albedos (Rowe et al. 2008). Despite their short periods, not all transiting exoplanets have been tidally circularized (Gillon et al. 2009a), and both rocky (e.g. CoRoT-Exo-7, $P \sim 0.85$ days) and gas giant (e.g. WASP-12b, $P \sim 1.09$ days) planets can exist in extremely short period orbits. Here, we report on the discovery of a new extreme transiting extra-solar planet with the shortest orbital period yet detected which is on the verge of spiraling into its host star. This transiting planet can not only inform us about the properties and evolution of close-in planets, but it also has the potential to provide information about the characteristics of its host star.

In this paper, we first describe all the observations that were obtained to detect and analyse the transiting star-planet system (§2). We describe the data analysis in §3 where we present the planet and its host star. Finally in §4, we discuss the implications of the planet’s short period and its future evolution.

2. Observations

2MASS J09534008-4539330 (hereafter WASP-19) is an apparently unremarkable 12th magnitude ($V = 12.59$), G8V star in the southern hemisphere located at $\alpha = 09:53:40.08$, $\delta = 45:39:33.0$ (J2000). The target was observed with the WASP-South telescope and instrumentation (Pollacco et al. 2006; Wilson et al. 2008) in the winter and spring observing seasons from 2006 to 2008. 1496 photometric data points were obtained between 4 May - 20 June 2006, 6695 measurements were made between 18 Dec 2006 - 18 May 2007, and 8968 observations were taken from 18 Dec 2007 - 22 May 2008. All data sets were processed independently with the standard WASP data reduction pipeline and photometry package (Collier Cameron et al. 2006). The individual data points have typical uncertainties of ~ 0.02 mags including poisson noise and systematic noise. The resulting light curves were then run through our implementation of the box least squares algorithm (Kovács et al. 2002) designed to detect periodic transit-shaped dips in brightness.

The target was initially flagged as a transiting planet candidate because a strong periodic signal was detected in the the 2007 data. The phase-folded light curve showed a square-shaped dip in brightness with a depth, $\delta \sim 25$ mmag and duration, $\tau \sim 1.2$ hours, consistent with a planet sized object around a main sequence star. Further, a periodic transit was also apparent in the 2006 data when phase-folded with the 2007 ephemeris, and a transit was subsequently detected in the 2008 season of data. Therefore, we classified the object as needing follow up photometry and

spectroscopy to assess the planetary nature of the system. The phase-folded light curve containing all WASP-South data is shown in Figure 1.

WASP-19 was observed photometrically with the 2m Faulkes Telescope South (FTS) on 17 December 2008 during transit. 139 Pan-STARRS z-band¹ observations were made over 3.3 hours. The images were observed in 2×2 binning mode such that one binned pixel corresponds to $0.279''$. They were processed in the standard way with IRAF using a stacked bias image, dark frame, and sky flat. Minimal fringing was present in the z-band images due to the deep depletion CCD in the camera, so no fringe correction was applied. The DAOPHOT photometry package (Stetson 1987) was used to perform object detection and aperture photometry with an aperture size of 8 binned-pixels in radius. The $5' \times 5'$ field-of-view of the instrument contained 53 comparison stars that were used in deriving the differential magnitudes with a photometric precision of 1.3 mmag. We measured the red noise (Pont et al. 2006) in the light curve on a 30 minute timescale to be 449 ppm and added this value in quadrature to the formal uncertainties on each data point. The resulting light curve is shown in Figure 2.

Thirty-four radial velocity measurements were obtained with the CORALIE spectrograph on the 1.2m Euler telescope (Baranne et al. 1996; Wilson et al. 2008). The stable, temperature controlled, high-resolution echelle spectrograph has a resolution of $R \sim 55000$ over the spectral region from $3800 - 6800 \text{ \AA}$. The WASP-19 spectra, obtained between 29 May 2008 and 23 April 2009, were processed through a slightly updated version of the CORALIE data reduction pipeline. In addition to the standard pipeline described in Baranne et al. (1996), we corrected for the blaze function and scaled the fitted cross-correlation region to match the full-width half maximum of the object. The final radial velocity (RV) values were obtained by cross-correlating the spectra with a G2 template mask. Table 1 presents the radial velocity measurements of WASP-19 at each Barycentric Julian date, the 1σ Poisson errors on the velocities, and the line bisector span measurements (Gray 1988; Queloz et al. 2001). Based on our experience, we adopt uncertainties on the line bisector measurements of twice the measured RV errors.

The radial velocity of the star varies sinusoidally with the same period measured from the photometry (see Figure 3). In addition, the line bisector spans, which are used to discriminate spot induced velocity variations and the effects of line-of-sight binarity, show no correlation with radial velocity within the uncertainties. The slope of the bisector versus RV (Figure 4) is -0.006 ± 0.037 , and the bisector measurements have an r.m.s. scatter of $\sim 50 \text{ m s}^{-1}$.

Although all existing photometric and spectroscopic data suggests WASP-19 is orbited by a short period transiting extra-solar planet, we explore the possibility of a false positive detection. In general, it is difficult to mimic the photometric and spectroscopic observations of a transiting planet without showing a visible second star in the spectrum, a significant bisector trend, and/or inconsistencies between the transit duration and host star spectral type. Starspots can cause periodic

¹<http://pan-starrs.ifa.hawaii.edu/public/design-features/cameras.html>

Table 1: Radial velocity measurements of WASP-19 obtained with the CORALIE spectrograph.

BJD	Vr km s ⁻¹	σ_{RV} km s ⁻¹	Bisector km s ⁻¹
2454616.46326	20.965	0.0218	-0.02975
2454623.46713	20.712	0.0289	0.03735
2454624.46191	21.019	0.0220	0.00607
2454652.46587	20.512	0.0210	0.02176
2454653.46543	20.770	0.0231	-0.03106
2454654.46530	21.007	0.0219	0.03017
2454656.47564	20.511	0.0193	-0.04093
2454657.46805	20.902	0.0386	0.04432
2454658.46376	21.008	0.0302	0.05792
2454660.46652	20.604	0.0400	0.05038
2454661.46434	20.974	0.0217	0.04052
2454662.46549	20.922	0.0191	0.01634
2454663.46607	20.547	0.0188	-0.02782
2454664.46573	20.645	0.0362	-0.14578
2454665.46709	21.077	0.0305	-0.00590
2454827.74752	20.683	0.0188	0.02320
2454832.74362	21.050	0.0242	-0.08001
2454833.66844	20.860	0.0212	0.01644
2454834.67693	20.548	0.0191	-0.04711
2454837.67024	20.726	0.0227	0.06777
2454838.68496	20.562	0.0244	-0.04762
2454839.70064	20.936	0.0185	-0.08634
2454890.61491	20.637	0.0187	0.00276
2454894.68743	20.518	0.0290	-0.02356
2454895.69238	20.894	0.0179	0.01631
2454896.66180	21.041	0.0145	-0.03853
2454897.65715	20.674	0.0175	-0.04530
2454898.66015	20.544	0.0197	-0.02811
2454939.53373	20.578	0.0164	-0.01384
2454940.52747	20.642	0.0154	0.03494
2454941.53928	20.996	0.0156	0.02525
2454942.52421	20.899	0.0169	-0.08243
2454943.53594	20.559	0.0191	0.05531
2454944.52955	20.798	0.0155	-0.02327

low-amplitude RV variations (e.g. Huélamo et al. 2008; Desort et al. 2007) but not photometric transits as well, thus a single star blended with a fainter stellar eclipsing binary (EB) is the preferred false positive scenario for transiting planets. Unfortunately, no comprehensive simulations have been performed which model the expected RV variations, eclipse shapes, and bisector slopes for different blended EB scenarios, and performing such simulations is beyond the scope of this discovery paper. Instead, we explore the blended EB scenario through qualitative reasoning.

In order to produce a flat-bottomed, 2% transit, as seen for WASP-19, the flux ratio of the EB compared to WASP-19 would have to be small enough that the EB was undetectable as a peak in the cross-correlation function. However, it could not be so small that the necessary unblended eclipse depth would require nearly equal sized EB components and therefore, a V-shaped eclipse (i.e. $0.05 < F_{EB}/F_{W19} < 0.2$). Although the eclipsing star would have to be small (and presumably less massive) compared to its primary to create the flat-bottomed eclipse, the RV amplitude of the visible EB primary would still be 40-90 km s⁻¹ for all reasonable mass ratios due to the high inclination angle needed to eclipse, the short orbital period of the observed transits, and the relatively deep transit (i.e. brown dwarf mass eclipsing objects would produce much shallower transit depths). Therefore, the RV variations of the EB could not be hidden within the WASP-19 spectral features given the resolution of the CORALIE data.

Furthermore, a short period stellar EB would almost certainly be tidally synchronized with $v \sin i \sim 40 - 80$ km s⁻¹. In the analysis of HD 41004 A (Santos et al. 2002), which exhibits planet-like RV variations due to a blended M dwarf + brown dwarf spectroscopic binary (SB), the bisector correlation is most dependent on the width of the visible SB component. This system, in which the SB is only 3% as bright as the single star and the width of the SB cross correlation function is ~ 8 km s⁻¹, shows a significant bisector correlation (slope of 0.67). According to their simulations, higher rotational broadening would produce an even greater bisector slope. Therefore, we would expect WASP-19 to show a significant bisector trend if the RV signal was caused by a rapidly rotating, blended EB, rather than a transiting planet.

Finally, we see no difference in the eclipse depth of the z-band FTS transit compared the SuperWASP transit taken in a bluer, V+R filter. Although this is not a strong constraint given the scatter in the SuperWASP photometry, an eclipse by a stellar object could show eclipse depth variations in different filters which we do not see. In summary, we conclude that the existing photometric and radial velocity variations of WASP-19 are most likely due to the presence of a transiting extra-solar planet.

3. Analysis

A combined analysis of the radial velocity curve and light curve of a transiting planet host star will provide direct measurements of the mass and radius of its orbiting planet with one additional constraint, e.g. the stellar mass. Below, we describe the determination of the stellar mass and other

host star properties.

3.1. Spectroscopic parameters

The individual CORALIE spectra were co-added into a single higher signal-to-noise (S/N) spectrum which was then used to measure the stellar temperature, gravity, metallicity, $v \sin i$ and elemental abundance information through comparisons with the synthetic spectra of Castelli et al. (1997). The results of the analysis are listed in Table 2. The quoted uncertainties directly correlate with the modest signal-to-noise of the co-added spectrum (S/N ~ 70).

The spectral synthesis technique is described in detail in Gillon et al. (2009a), therefore we only give a short summary here. The H α line was the primary temperature determinant, while the Na I D and Mg I b lines were used as surface gravity ($\log g$) diagnostics. By measuring the equivalent width of several clean and unblended metal lines, we derived abundances for the elements listed in Table 2. Due to the spread in abundance measurements, we adopt an overall metallicity for the system of $[M/H] = 0.1 \pm 0.1$. The microturbulence ($1.1 \pm 0.2 \text{ km s}^{-1}$), which directly affects the abundance measurements, was derived from the Fe I lines using Magain’s (1984) method.

The projected rotational velocity ($v \sin i$) was determined by fitting the profiles of several unblended Fe I lines. We accounted for line broadening due to the instrumental FWHM (0.11 \AA) which was determined from telluric lines around 6300 \AA , and the macroturbulence (2 km s^{-1}) which was based on the tabulation by Gray (2008). Finally, we do not detect Li I in the stacked spectrum, and can therefore only put an upper limit on the abundance of this element of $\log A(\text{Li}) < 1$.

3.2. Host star mass

By comparing the effective temperature, metallicity, and mean stellar density (ρ_*) of WASP-19 to theoretical stellar models, we determine its mass. The stellar density is dependent on the shape of the transit and largely independent of any assumptions or models (Seager & Mallén-Ornelas 2003). Thus, after deriving the spectroscopic parameters, we model the WASP-South and FTS transit light curves of WASP-19 using the Markov-chain Monte Carlo (MCMC) routine described in Collier Cameron et al. (2007) to derive the stellar density and its uncertainty. The code uses the MCMC approach to simultaneously solve for the orbital and physical properties of the star-planet system. We apply the limb darkening coefficients of Claret (2000, 2004) for the appropriate temperature of the star and wavelength of the light curves. We note that the eccentricity value has an effect on the stellar density determination, thus we first allow the eccentricity to be a free parameter. Since the resulting eccentricity value gives a non-significant 1.5σ detection, we solve for the stellar density a second time while fixing the eccentricity to be zero.

Interpolating among the Girardi et al. (2000) stellar evolution tracks as described in Hebb et al.

Table 2: Stellar properties of WASP-19 obtained from the NOMAD catalogue and derived from our analysis of the spectra and light curves.

Parameter	WASP-19
RA(J2000)	09:53:40.08
Dec(J2000)	-45:39:33.0
J	10.911 ± 0.026
H	10.602 ± 0.022
K	10.481 ± 0.023
μ_{RA}	$-41.3 \pm 2.5 \text{ mas yr}^{-1}$
μ_{DEC}	$16.5 \pm 1.9 \text{ mas yr}^{-1}$
U	$-49_{-15}^{+21} \text{ km s}^{-1}$
V	$-25_{-2}^{+2} \text{ km s}^{-1}$
W	$-13_{-10}^{+7} \text{ km s}^{-1}$
T_{eff}	$5500 \pm 100 \text{ K}$
$\log g$	4.5 ± 0.2
ξ_{t}	$1.1 \pm 0.1 \text{ km s}^{-1}$
$v \sin i$	$4 \pm 2 \text{ km s}^{-1}$
[Fe/H]	0.02 ± 0.09
[Si/H]	0.15 ± 0.07
[Ca/H]	0.12 ± 0.15
[Ti/H]	0.13 ± 0.12
[Ni/H]	0.10 ± 0.08
$\log A(\text{Li})$	$<1.$
ρ_*	$1.13 \pm 0.12 \rho_{\odot}$
P_{rot}	$10.5 \pm 0.2 \text{ days}$

(2009), we derive a mass for the host star of $M_* = 0.95_{-0.10}^{+0.09} M_\odot$ using the circular orbit solution. The non-circular orbit value for the stellar density results in a mass of $0.96 M_\odot$, well within the existing error bars (adopted from the non-circular solution). Figure 5 shows a plot of the position of WASP-19 in a modified Hertzsprung-Russell diagram as compared to the theoretical tracks. The errors on the stellar mass are dominated by the uncertainty on the metallicity. Here, we take into account uncertainties on the stellar temperature, metallicity and density. We do not include systematic uncertainties on the chosen stellar model which are difficult to determine, but we might expect this additional uncertainty to be at least $\sim 4\%$. Southworth (2009) finds that with stellar parameters measured at the limit of our technological and theoretical ability for HD 209458b, the variation in the mass determination using four different stellar models is $\sim 4\%$.

3.3. Host star age

The isochrone fitting also allows for deriving an age estimate for WASP-19. According to these stellar models, WASP-19 is a main-sequence star with an age of $5.5_{-4.5}^{+9.0}$ Gyr when we adopt the zero eccentricity value for the stellar density. This essentially places a weak constraint on the stellar age to be $\gtrsim 1$ Gyr. If we adopt the value for the stellar density from the solution when the eccentricity is a free parameter (non-significant 1.5σ result), we are unable to place any constraints on the stellar age from the isochrones. The depletion of lithium in the atmosphere of a G8V star can also be used as an age indicator. However, the non-detection of Li I in WASP-19 again gives only a weak constraint on the age suggesting the star is older than the Hyades (0.6 Myr, Sestito & Randich 2005).

We, therefore, examine the three dimensional velocity of WASP-19 as compared to theoretical Galactic model stars to estimate the probability that WASP-19 is part of a young disk population. Using the catalogue proper motions and measured systemic radial velocity, we calculate its U , V , and W space motion (given in Table 2) compared to the Sun. We estimate the distance of WASP-19 to be 250_{-60}^{+80} pc using the measured spectral type, G8V, with absolute magnitude, $M_v = 5.6$ from Gray (1988) and V magnitude from the NOMAD catalogue ($V = 12.59$). We adopt a ± 0.2 uncertainty on the magnitude measurement as it is not given in the catalogue and a generous error of ± 2 subclasses in spectral type to determine the uncertainty on the distance estimate. We select a set of model main sequence stars of spectral types F7-K7 in a small volume around WASP-19 ($l = 273 \pm 3^\circ$, $b = 7 \pm 3^\circ$, distance=150-400 pc) using the Besançon Galactic model (Robin et al. 2003). We generate 100 realizations of the simulation which provide the heliocentric velocities, metallicities, and population classes for over 500,000 model stars. Of the model stars with metallicities of 0.0-0.2 dex and with space motions within the errors of the calculated U, V , and W values of WASP-19, 35% of the model stars have ages of < 1 Gyr (population class 1 and 2), 59% have ages of 1-5 Gyr (population class 3-5) and 6% have ages of 5-10 Gyr. Contributions from the thick disk, halo and bulge populations are negligible. This analysis suggests WASP-19 has a 65% probability of being older than 1 Gyr.

In summary, we present three different age dating techniques which all suggest WASP-19 is older than ~ 1 Gyr, however a precise age for the star cannot be determined from the existing data.

3.4. Host star rotation period

We search for variability in the WASP-South light curves of WASP-19 caused by asymmetric starspots on the photosphere which modulate the flux. Any starspots will rotate in and out of view with the stellar surface, such that the period of the variability gives the rotation period of the star. To exhibit rotational variability, the star must have a sufficient coverage of starspots to create a variable brightness signal which is detectable given the scatter in the photometric data. Furthermore, starspots evolve on timescales of weeks or months causing the amplitude and phase of the variability to change, therefore, each season of WASP-South data was examined independently.

To detect the rotational variability, we determine the improvement in χ^2 over a flat, non-variable model when a sine wave of the form $y = a_0 + a_1 \sin(\omega t + a_3)$ is fit to each season of the WASP-South data phase-folded at a set of trial periods, $P_{rot} = 2\pi/\omega$. We subtract all transits from the light curves using the model derived from the parameters in Table 3 before fitting the sine curve model. We test periods between 0.2 – 50 days and find a strong periodic signal in the 2007 data with $P_{rot} = 10.5$ days and amplitude, $a_1 = 7.6$ mmag. The phase-folded light curve and periodogram of normalized $\Delta\chi^2$ values are shown in Figure 6 and Figure 7 (top), respectively. In the 2008 data, we also detect a weaker signal with a similar period, $P_{rot} = 10.6$ days, and with an amplitude of 3.6 mmag.

To assess the veracity of the sinusoidal signal detected in the 2007 data, we determine the significance and the false alarm probability (FAP) following Zechmeister & Kürster (2009) (employing the residual variance normalization). The equations include, N , the number of independent data points, and M , the number of independent frequencies, as well as the measured peak value in the periodogram. According to Cumming (2004), the number of independent frequencies can be approximated by the duration of the time-series data times the difference between the highest and lowest frequencies tested (here $M = 753$). The number of independent data points depends on the level of red noise in the light curve. We empirically determine N by generating a new light curve in which the red noise is preserved, but the periodic signal is destroyed. We randomly re-order the individual nights of data, so that the integer part of the light curve time values are shuffled, but the fractional parts (containing the red noise) remain the same. We then run the sine fitting program on the shuffled light curve and find $N = 664$ by assuming the highest peak in the resulting periodogram (Figure 7 (bottom)) has a 95% probability of being false ($FAP = 0.95$). Using our calculated N and M , we then apply the equations in Zechmeister & Kürster (2009) to the results of the sine fitting on the original 2007 light curve and find a highly significant periodic signal with a $\text{Prob}(p > p_{\text{best}}) = 1.4 \times 10^{-10}$ and $FAP = 1 \times 10^{-7}$. Thus, we adopt a rotation period for WASP-19 of $P_{rot} = 10.5$ days.

We calculate the error on this measurement using the formula in Horne & Baliunas (1986) and find $\sigma_P = 0.08$, but given the variation in period values we measure using two other techniques (Lomb-Scargle and auto-correlation), we find this to be underestimated and suggest $\sigma_P = 0.2$ days is a more realistic uncertainty. Finally, we note that the 10.5 day rotation period of the star measured via the photometry is consistent with the less precise $v \sin i$ value of $4 \pm 2 \text{ km s}^{-1}$ which corresponds to a rotational period of between 8-24 days (assuming the spin axis of the star is perfectly aligned with the orbital axis).

The rotation period of a main sequence star can also be used to estimate its age. According to the Barnes (2007) gyrochronology relationship, a rotation period of $P_{rot} = 10.5$ days corresponds to an age of 500-600 Myr for a G8V star like WASP-19 with B-V=0.74. This value is not consistent with the older age inferred from the isochrones, lithium, and space motion. In § 4, we discuss the implications of the possible discrepancy between the different age indicators.

3.5. Planet properties

We solved for the properties of the star-planet system by running an MCMC code (Collier Cameron et al. 2007) using as inputs the WASP-South light curve, the FTS light curve, the CORALIE radial velocity curve, and the stellar mass. Initially, we allowed the $e \cos \omega$ and $e \sin \omega$ to be free parameters, but the low, non-zero values that resulted were not significant. Therefore, we also solved for the parameters of the system while forcing the planet to be on a circular orbit. The difference in stellar and planet properties derived for the circular and non-circular orbit cases is negligible and within the 1σ uncertainties on all parameters. However, for completeness, we provide the resulting solutions for both cases. Table 3 gives the final model parameters for the transit and radial velocity curves as well as the physical properties of the star-planet system.

Note, we do not remove the rotational variability from the light curves before deriving the final system parameters. The model fit is dominated by the FTS data, and the low-amplitude 10.5 day rotational variability is negligible on the 3.3 hour timescale of this light curve. We confirm this by fixing the orbital period to the value found when analysing all the light curve data and fitting just the FTS light curve and radial velocity data. All the resulting light curve parameters and physical system parameters are well within their reported 1σ uncertainties. Therefore, we do not ‘pre-whiten’ the WASP-South data before performing the final transit model fits on all the existing photometric data. However, it is important to note that we cannot determine if any starspots were present on WASP-19 during the FTS observations which might affect the resulting parameter determinations because of the relatively small amount of out-of-transit data. Additional high quality transit data would allow for investigating any variations in the derived parameters due to starspots.

Finally, to derive the final parameters, we use the 4-coefficient limb darkening model by Claret (2004, 2000) with the ATLAS model atmospheres, an effective temperature of 5500 K, and a log g of

4.5. However, we tested a range of limb darkening coefficients with different temperatures, $\log g$ values, and model atmospheres and found the resulting parameters to be highly robust to changes in these coefficients. We suspect this is due to the fact the FTS z-band data dominates our parameter results, and this filter is not as susceptible to limb darkening uncertainties as bluer filter data.

3.6. Transit Timing

We measured the heliocentric Julian date of the mid-transit times for WASP-19b using the technique described in Anderson et al. (2009) to search for variations which could indicate the presence of a outer planet (e.g. Agol et al. 2005). In general, the SuperWASP transits are not precise enough to provide a useful constraint on the existence of a third body in the system, but these data do rule out transit timing variations larger than ~ 15 minutes.

4. Discussion

The most striking aspect of WASP-19b is its extremely short orbital period. With a period, $P = 0.7888399 \pm 0.0000008$ days, WASP19b is the shortest period planet yet discovered. What physical processes in the evolution of the planet have lead to such a close separation? Did the initial migration process leave the planet in its extremely short period orbit or has there been subsequent evolution of the orbital separation? The observations presented here suggest the possibility that WASP-19b has been spiralling into its host star throughout its lifetime and has spun up its host star in the process.

Most transiting extrasolar planets will ultimately spiral into their host stars because there is insufficient total angular momentum in the systems to reach a state of tidal equilibrium (Hut 1980; Rasio et al. 1996; Jackson et al. 2009). However, the timescale for this evolution is not well known because the stellar tidal quality factor, Q'_s , is uncertain to at least three orders of magnitude. Values between $10^6 < Q'_s < 10^9$ are reasonable (Jackson et al. 2008, and references therein). Furthermore, the planetary tidal quality factor, Q'_p is equally uncertain, but it affects the evolution of the stellar spin and planetary orbital separation to a much lesser degree.

For WASP-19b, the ratio of total to critical angular momentum is well below the limiting value of one, thus ensuring the planet will ultimately collide with its host star, but the lifetime of this evolution ranges from 4 Myr to 4 Gyr depending on the value used for Q'_s . However, unlike most other transiting planets, we have measured the rotation period of WASP-19 which contributes additional information that can be used to place tighter constraints on the overall lifetime of the planet and on the tidal quality factor of the star.

By integrating the coupled equations of orbital eccentricity and separation (Dobbs-Dixon et al. 2004) while conserving the total angular momentum of the system, we can model the future evo-

Table 3: WASP-19 system parameters and 1σ error limits derived from the MCMC analysis.

Parameter	Symbol	Value (e fixed)	Value (e free)	Units
Transit epoch (BJD)	T_0	$2454775.3372^{+0.0001}_{-0.0002}$	$2454775.3372^{+0.0002}_{-0.0002}$	days
Orbital period	P	$0.7888399^{+0.0000008}_{-0.0000008}$	$0.7888399^{+0.0000008}_{-0.0000008}$	days
Planet/star area ratio	$(R_p/R_s)^2$	$0.0203^{+0.0004}_{-0.0004}$	$0.0203^{+0.0004}_{-0.0004}$	
Transit duration	t_T	$0.0642^{+0.0006}_{-0.0006}$	$0.0643^{+0.0006}_{-0.0007}$	days
Impact parameter	b	$0.62^{+0.03}_{-0.03}$	$0.62^{+0.03}_{-0.03}$	R_*
Stellar reflex velocity	K_1	$0.256^{+0.005}_{-0.005}$	$0.256^{+0.005}_{-0.005}$	km s ⁻¹
Centre-of-mass velocity	γ	$20.78534^{+0.0002}_{-0.0002}$	$20.78535^{+0.0003}_{-0.0003}$	km s ⁻¹
Orbital semimajor axis	a	$0.0165^{+0.0005}_{-0.0006}$	$0.0164^{+0.0005}_{-0.0006}$	AU
Orbital inclination	I	$80.5^{+0.7}_{-0.7}$	$80.8^{+0.8}_{-0.8}$	degrees
Orbital eccentricity	e	0 (fixed)	$0.02^{+0.02}_{-0.01}$	
Longitude of periastron	ω	0 (fixed)	-76^{+112}_{-23}	deg
eccentricity \times cos(ω)	$e\cos\omega$	0 (fixed)	$0.004^{+0.009}_{-0.009}$	
eccentricity \times sin(ω)	$e\sin\omega$	0 (fixed)	$-0.02^{+0.02}_{-0.02}$	
Stellar mass	M_*	$0.96^{+0.09}_{-0.10}$	$0.95^{+0.10}_{-0.10}$	M_\odot
Stellar radius	R_*	$0.94^{+0.04}_{-0.04}$	$0.93^{+0.05}_{-0.04}$	R_\odot
Stellar surface gravity	$\log g_*$	$4.47^{+0.03}_{-0.03}$	$4.48^{+0.03}_{-0.03}$	[cgs]
Stellar density	ρ_*	$1.13^{+0.09}_{-0.09}$	$1.19^{+0.12}_{-0.11}$	ρ_\odot
Planet radius	R_p	$1.31^{+0.06}_{-0.06}$	$1.28^{+0.07}_{-0.07}$	R_J
Planet mass	M_p	$1.15^{+0.08}_{-0.08}$	$1.14^{+0.07}_{-0.07}$	M_J
Planetary surface gravity	$\log g_p$	$3.19^{+0.03}_{-0.03}$	$3.20^{+0.03}_{-0.03}$	[cgs]
Planet density	ρ_p	$0.51^{+0.06}_{-0.05}$	$0.54^{+0.07}_{-0.06}$	ρ_J
Planet temperature ($A = 0, F=1$)	T_{eq}	2009^{+26}_{-26}	1993^{+32}_{-33}	K

lution of the planet as it spirals inward and further spins up the host star. In the analysis, we include magnetic braking which takes the form $\dot{\Omega} = -\kappa\Omega^3$ with $\kappa = 3.88 \times 10^{-7}$ s as evaluated using equation (12) of Collier Cameron & Jianke (1994). We use the current orbital separation derived from the MCMC analysis (Table 3) and the measured rotation period ($P_{rot} = 10.5$ days) as initial conditions. Figure 8 shows the future evolution of the planet in orbital separation, and in Figure 9, we plot the corresponding rotational evolution of the star.

The results show that in the $Q'_s = 10^9$ case, the tidal interaction is so weak that the star's future evolution is dominated by magnetic braking. In this situation, the relatively short rotation period could not have been caused by prior tidal interactions with the planet and would instead suggest a young stellar age similar to that of the Hyades (~ 600 Myr). Although it is possible WASP-19 is as young as the Hyades, the isochrones analysis, the non-detection of lithium, and the stellar velocity all favor an older age for the star. Therefore, a lower value for Q'_s is preferred.

For all models with $Q'_s < 10^8$, the star's spin period has already passed through a maximum and is decreasing as the planet spirals in. However, in the $Q'_s = 10^6$ case, the remaining lifetime of the planet is extremely short (4 Myr). Therefore, the existing data appears to favor values of $Q'_s = 10^7 - 10^8$ which are high enough to give significant life expectancy, but low enough to have reversed magnetic braking and initiated spiral-in. This scenario would allow for the extremely short period of the planet to be a consequence of further evolution in orbital separation after the initial migration process early in its formation and evolution. However, the Q'_s would have to be 1-2 orders of magnitude greater than the nominal value of 10^6 that is typically adopted (e.g. Bodenheimer et al. 2003; Jackson et al. 2008).

It is important to note that Q'_s is a simple parameterization of the complex physics involving the interaction between the tides raised by the planet on its star and the turbulent viscosity in the stellar convection zone and inertial wave modes excited in the stellar interior (Rasio et al. 1996; Sasselov 2003; Ogilvie & Lin 2007). A more detailed analysis of this system and others like it (e.g. WASP-18, OGLE-TR-56b, WASP-12) will hopefully lead to a better understanding of the physics modulating tidal dissipation in stars, since currently, there is no comprehensive theory which is able to explain observations of both main sequence binary stars and close-in extra-solar planets with regard to their tidal evolution (Rasio et al. 1996; Sasselov 2003; Terquem 1998; Ogilvie & Lin 2007).

Finally, we note that the stellar flux incident on WASP-19b at the substellar point is 3.64×10^9 ergs cm⁻² s⁻¹ placing it in the class of highly irradiated planets like OGLE-TR-56b (Konacki et al. 2003; Torres et al. 2004) and WASP-1b (Cameron et al. 2007). Therefore, we expect the planet to have large secondary eclipse depths in the mid-IR, evidence of an atmospheric temperature inversion, molecular emission features, and a large day/night contrast (Fortney et al. 2008). The existence of a hot stratosphere can be tested using secondary eclipse measurements that are currently being obtained with Spitzer. Eclipse measurements in the near-IR and optical z-band are also possible given current technology (e.g. Gillon et al. 2009b). Furthermore, the density of WASP-19b

is half that of Jupiter’s ($\rho_p = 0.51\rho_J$), so it is slightly bloated for its mass, but not extremely so. The high irradiation, increased metallicity of the host star, and dissipation of tidal energy are possible factors causing the enhanced radius (Bodenheimer et al. 2003; Fortney et al. 2007; Burrows et al. 2007).

In summary, WASP-19b is the shortest period transiting planet yet detected. It has a mass, $M_{\text{pl}}=1.15 M_J$ and radius, $R_{\text{pl}}=1.31 R_J$. The planet orbits a main sequence G-dwarf with a slightly super-solar metallicity and a rotation period of $P_{\text{rot}} = 10.5 \pm 0.2$ days. It is likely WASP-19b has been spiraling into its host star over its lifetime and has spun up the star in the process. A more precise age determination of WASP-19 will allow us to confirm this and to place stronger constraints on the star’s tidal quality factor, Q'_s .

The SuperWASP Consortium consists of astronomers primarily from the Queen’s University Belfast, St Andrews, Keele, Leicester, The Open University, Isaac Newton Group La Palma and Instituto de Astrofísica de Canarias. The SuperWASP Cameras were constructed and operated with funds made available from Consortium Universities and the UK’s Science and Technology Facilities Council.

REFERENCES

- Agol, E., Steffen, J., Sari, R., & Clarkson, W. 2005, MNRAS, 359, 567
- Anderson, D. R., et al. 2009, arXiv:0908.1553
- Baranne, A., et al. 1996, A&AS, 119, 373
- Barnes, S. 2007 ApJ, 669, 1167
- Bodenheimer, P., Laughlin, G., & Lin, D. N. C. 2003, ApJ, 592, 555
- Burrows, A., Hubeny, I., Budaj, J., & Hubbard, W. B. 2007, ApJ, 661, 502
- Cameron, A. C., et al. 2007, MNRAS, 375, 951
- Castelli F., Gratton R.G., Kurucz R.L., 1997, A&A 318, 841
- Claret A., 2000, A&A, 363, 1081
- Claret A., 2004, A&A, 428, 1001
- Collier Cameron, A., & Jianke, L. 1994, MNRAS, 269, 1099
- Collier Cameron A., et al., 2006, MNRAS, 373, 799
- Collier Cameron A., et al., 2007, MNRAS, 380, 1230

- Cumming, A. 2004, MNRAS, 354, 1165
- Desort, M., Lagrange, A.-M., Galland, F., Udry, S., & Mayor, M. 2007, A&A, 473, 983
- Dobbs-Dixon, I., Lin, D. N. C., & Mardling, R. A. 2004, ApJ, 610, 464
- Fortney, J. J., Marley, M. S., & Barnes, J. W. 2007, ApJ, 659, 1661
- Fortney, J. J., Lodders, K., Marley, M. S., & Freedman, R. S. 2008, ApJ, 678, 1419
- Gillon, M., et al. 2009, A&A, 501, 785
- Gillon, M., et al. 2009, A&A, 506, 359
- Girardi, L., Bressan, A., Bertelli, G., & Chiosi, C. 2000, A&AS, 141, 371
- Gray D.F., 2008, The observation and analysis of stellar photosphere s, 3rd Edition, CUP, p. 507.
- Gray D.F., 1988, Lectures on Spectral-line Analysis: F, G, and K Stars (Arva, Ontario: Publisher)
- Hebb, L., et al. 2009, ApJ, 693, 1920
- Horne, J. H., & Baliunas, S. L. 1986, ApJ, 302, 757
- Huélamo, N., et al. 2008, A&A, 489, L9
- Hut, P. 1980, A&A, 92, 167
- Jackson, B., Greenberg, R., & Barnes, R. 2008, ApJ, 678, 1396
- Jackson, B., Barnes, R., & Greenberg, R. 2009, ApJ, 698, 1357
- Knutson, H. A., Charbonneau, D., Allen, L. E., Burrows, A., & Megeath, S. T. 2008, ApJ, 673, 526
- Konacki, M., Torres, G., Jha, S., & Sasselov, D. D. 2003, Nature, 421, 507
- Kovács, G., Zucker, S., & Mazeh, T. 2002, A&A, 391, 369
- Magain, P. 1984, A&A, 132, 208
- Mandel K., & Agol E., 2002, ApJL, 580, L171
- Mayor, M., & Queloz, D. 1995, Nature, 378, 355
- Ogilvie, G. I., & Lin, D. N. C. 2007, ApJ, 661, 1180
- Pollacco, D., et al. 2006, PASP, 118, 1407
- Pont F, Zucker S., Queloz D. 2006, MNRAS, 373, 231

- Queloz D., et al. 2001, *A&A*, 379, 279
- Rasio, F. A., Tout, C. A., Lubow, S. H., & Livio, M. 1996, *ApJ*, 470, 1187
- Robin, A. C., Reyl e, C., Derri ere, S., & Picaud, S. 2003, *A&A*, 409, 523
- Rowe, J. F., et al. 2008, *ApJ*, 689, 1345
- Santos, N. C., et al. 2002, *A&A*, 392, 215
- Sasselov, D. D. 2003, *ApJ*, 596, 1327
- Sato, B., et al. 2005, *ApJ*, 633, 465
- Seager, S., & Mall en-Ornelas, G. 2003, *ApJ*, 585, 1038
- Sestito, P., & Randich, S. 2005, *A&A*, 442, 615
- Southworth, J. 2009, *MNRAS*, 394, 272
- Stetson P. 1987, *PASP*, 99, 191
- Terquem, C. E. J. M. L. J. 1998, *ApJ*, 509, 819
- Torres, G., Konacki, M., Sasselov, D. D., & Jha, S. 2004, *ApJ*, 609, 1071
- Wilson, D. M., et al. 2008, *ApJ*, 675, L113 Urban, S. E., Gaume, R., & Wycoff, G. L. 2004, *Bulletin of the American Astronomical Society*, 36, 1418
- Zechmeister, M., K urster, M. 2009, *A&A*, 496, 577

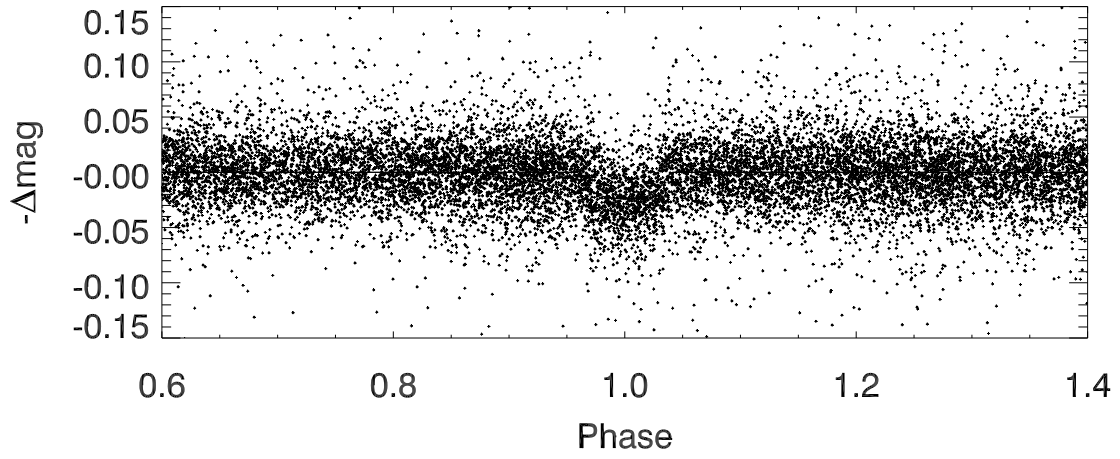


Fig. 1.— WASP-South discovery photometry of WASP-19. The data are phase-folded with the ephemeris given in Table 3.

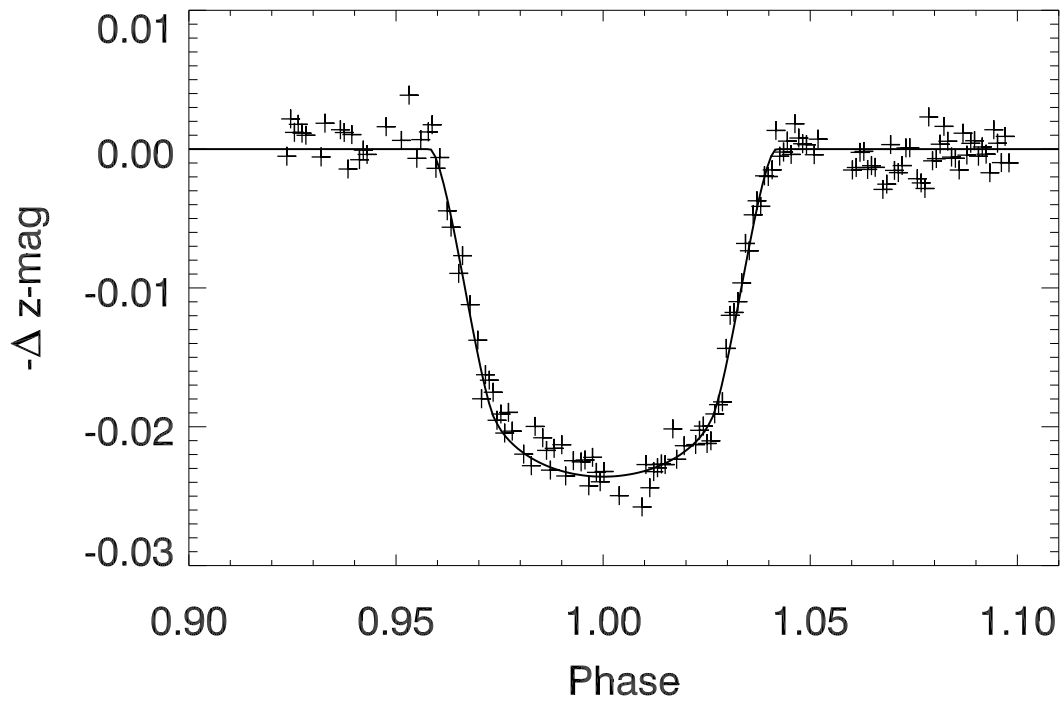


Fig. 2.— FTS z -band photometry of the WASP-19 transit. The data are converted to phase using the ephemeris given in Table 3. Overplotted is the best fitting model transit light curve using the formalism of Mandel & Agol (2002) applying the 4th-order limb darkening coefficients from Claret (2004).

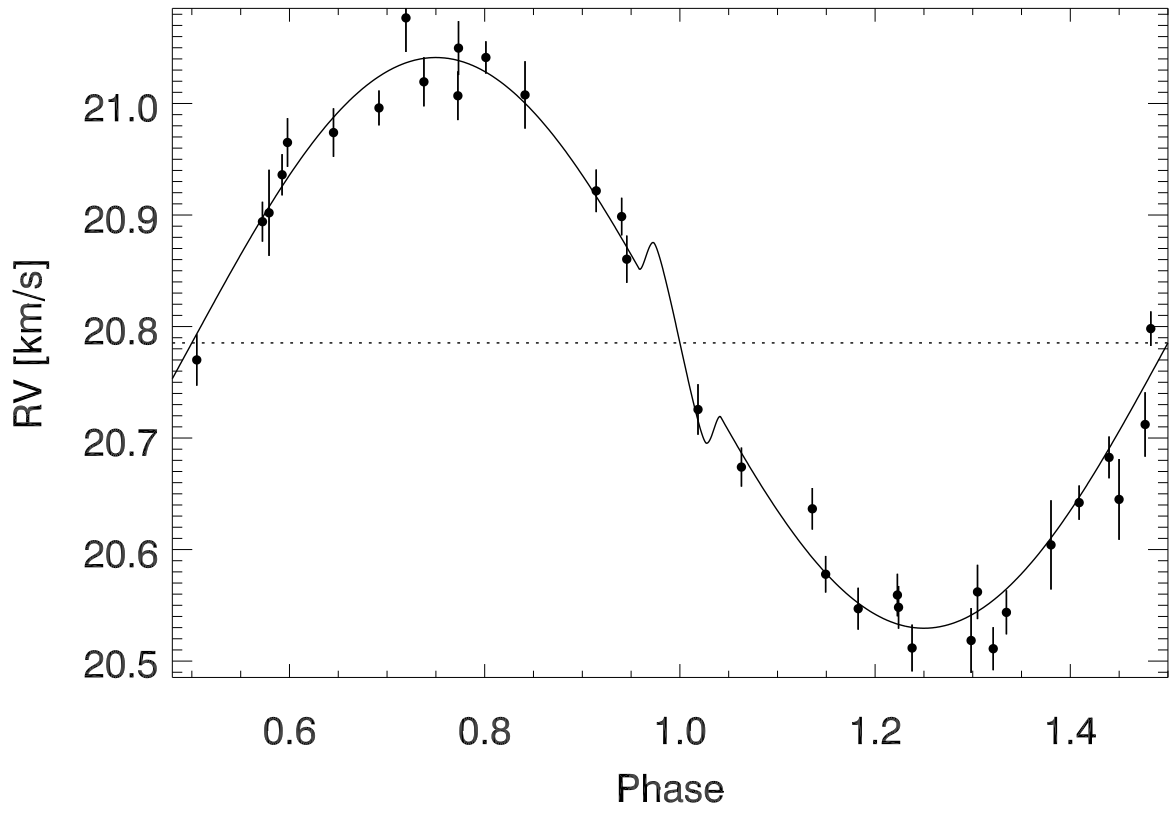


Fig. 3.— Radial velocity curve of WASP-19 phase-folded with the ephemeris given in Table 3. Overplotted is the best fitting model curve obtained from a combined analysis of the photometric and spectroscopic data.

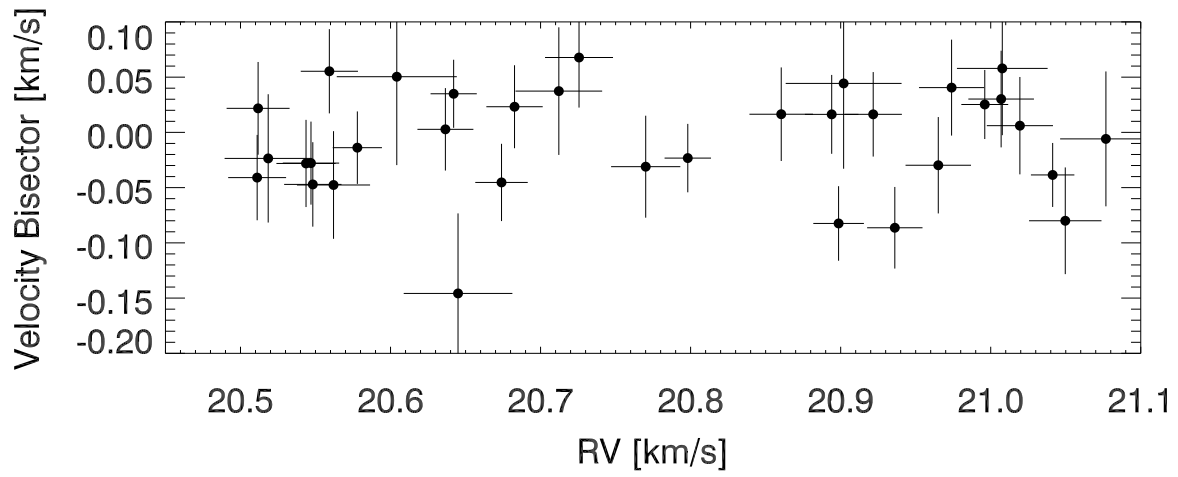


Fig. 4.— Line bisector span versus radial velocity. The uncertainties on the line bisector values are double the values on the radial velocity measurement. There is no correlation between the line bisector span measurements and radial velocity which rules out star spot variations or a blended eclipsing binary as the cause for the velocity variations.

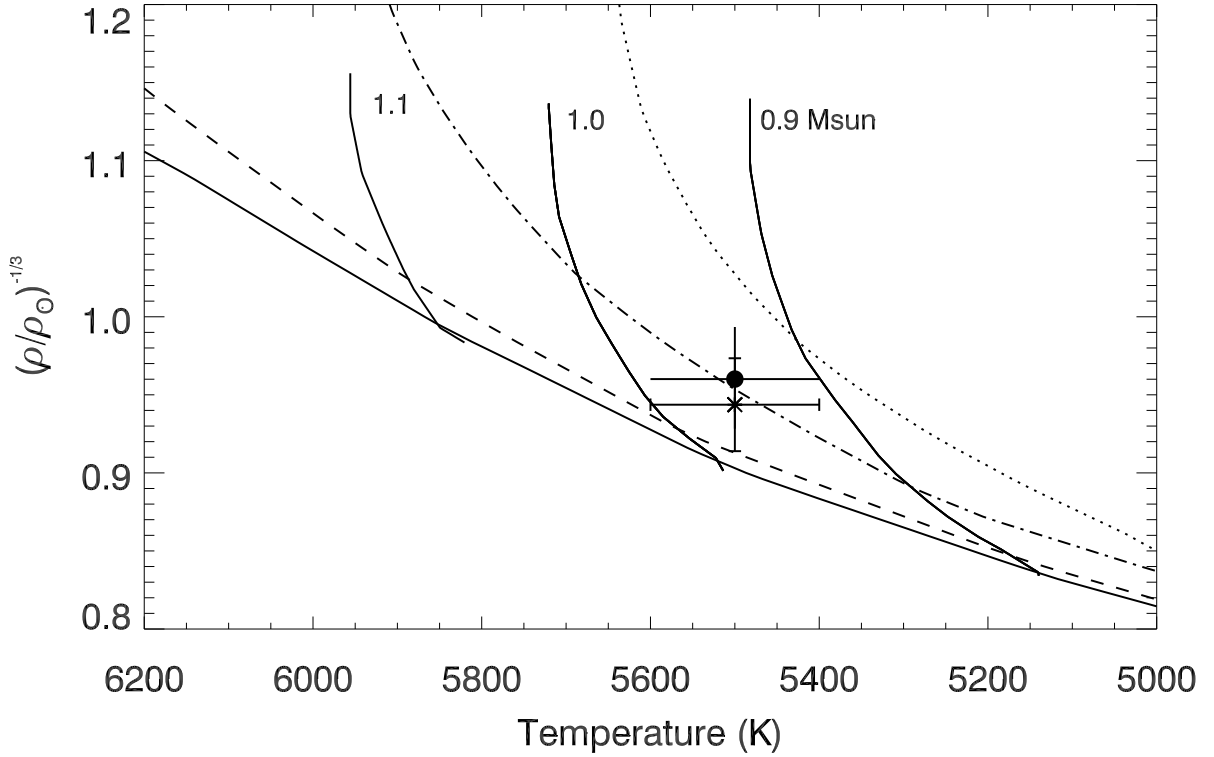


Fig. 5.— Modified Hertzsprung-Russell diagram comparing the stellar density and temperature of WASP-19 to theoretical stellar evolution tracks by Girardi et al. (2000) interpolated at a metallicity of $[M/H]=+0.1$. The solid circle shows the result when the eccentricity is zero, and the asteriks shows the value for the stellar density if the eccentricity is a free floating parameter. The mass tracks are labelled and the isochrones are 0.1 (solid), 1 (dashed), 5 (dot-dashed), and 10 (dotted) Gyr.

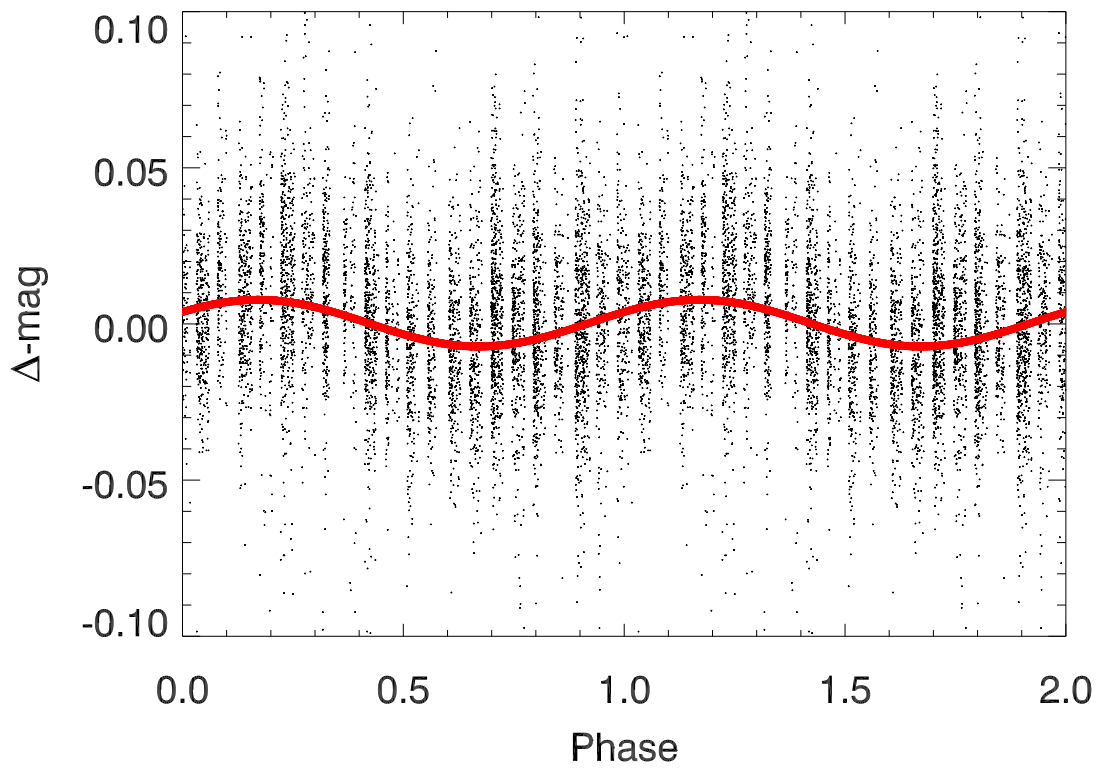


Fig. 6.— WASP-South light curve data from 2007 phase-folded on the rotation period detected in the sine fitting, $P_{rot} = 10.5$ days.

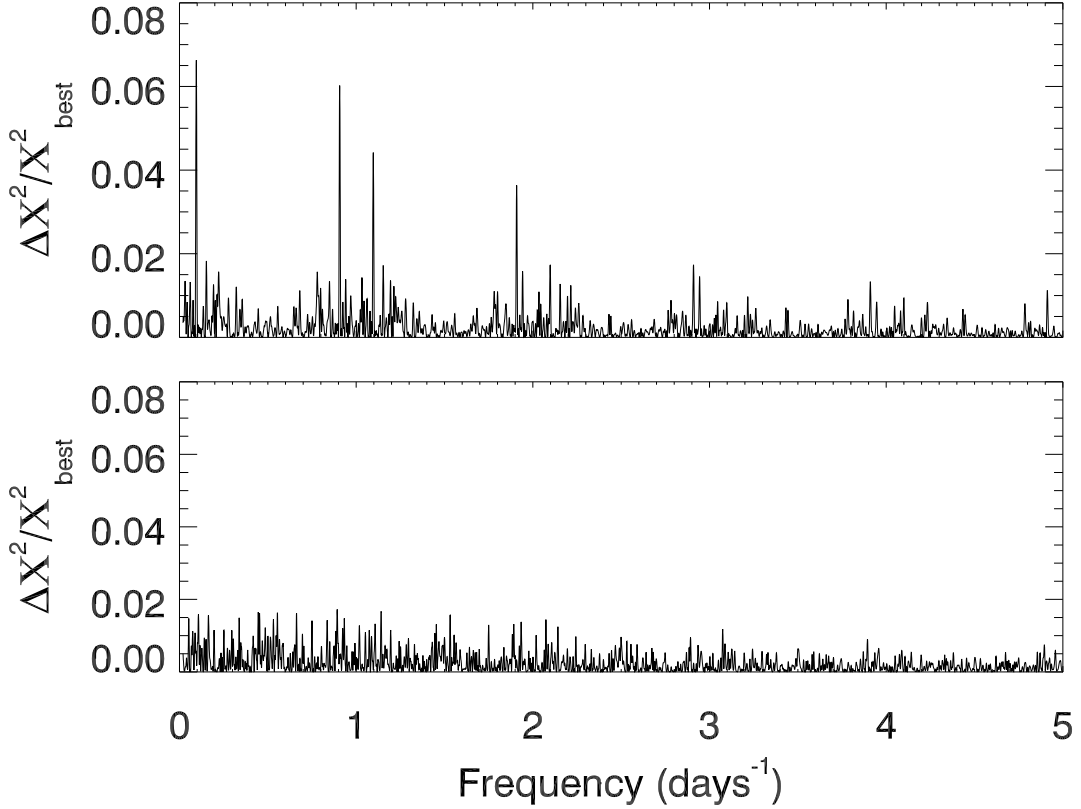


Fig. 7.— Top: Periodogram, $\Delta\chi^2/\chi_{best}^2$ versus frequency, resulting from fitting a sine wave to the 2007 WASP-South light curve. The peak in the periodogram has a $FAP = 1 \times 10^{-7}$ and occurs at $P_{rot} = 10.5$ days indicating the rotation period of the star. Bottom: Periodogram resulting from fitting a sine wave to the shuffled 2007 light curve in which the periodic signal was destroyed, but the red (Pont et al. 2006) and white noise were preserved. We adopted a $FAP = 0.95$ for the highest peak.

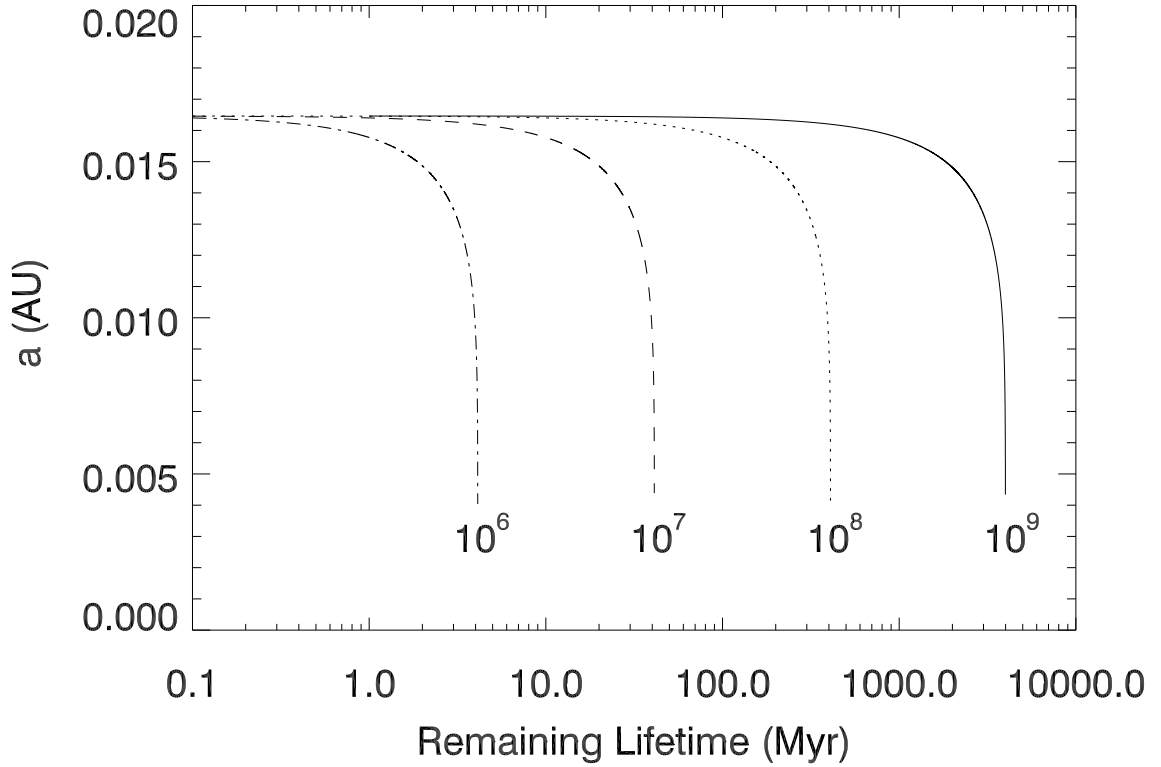


Fig. 8.— Orbital separation versus age of WASP-19b when evolved forward from the current state to the point when the planet overflows its Roche lobe. Due to exchange of angular momentum through tides, the planet loses orbital angular momentum and spirals into the star. The different lines which are labelled correspond to different values for the stellar quality factor, Q'_s . The remaining lifetime of the planet ranges from 4 Myr to 4 Gyr depending on the value of Q'_s .

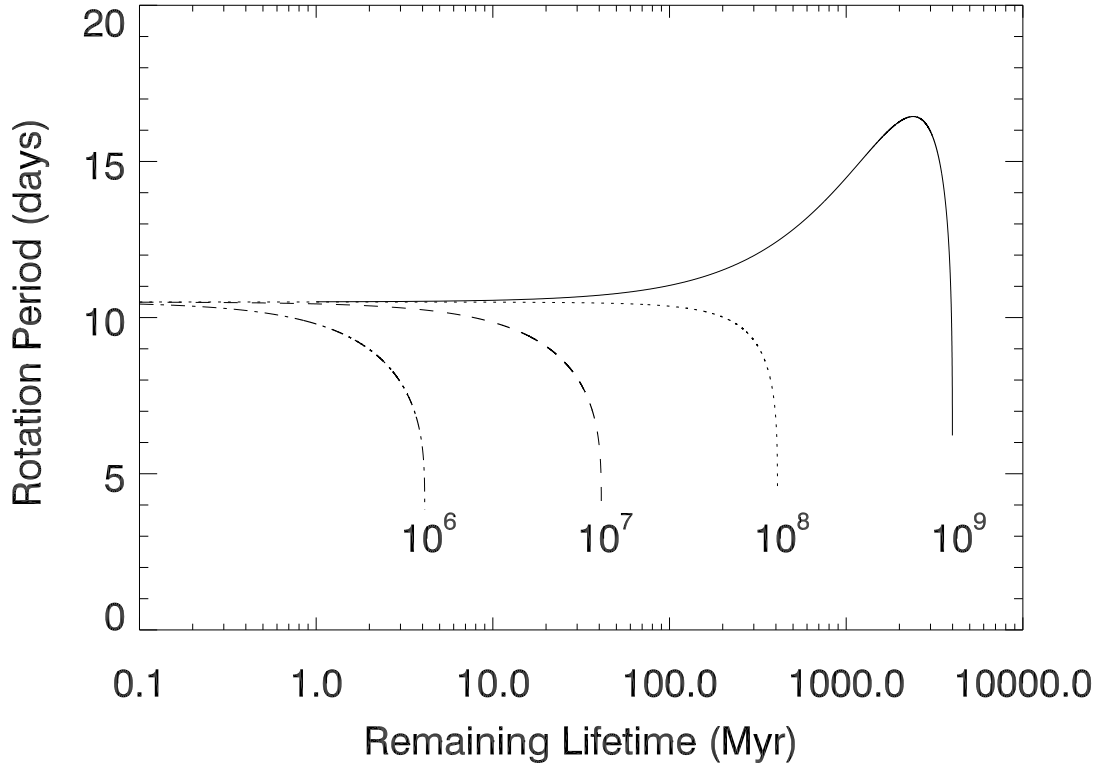


Fig. 9.— Stellar rotation versus age of WASP-19b when evolved forward accounting for tidal evolution. The star gains rotational angular momentum and spins up as the planet spirals into the star, losing angular momentum. The different lines are labelled for different values of Q'_s . For $Q'_s = 10^9$, the tidal evolution is slow enough that magnetic braking due to stellar winds dominates the angular momentum of the star causing it to slow down prior to the eventual spiral in of the planet after ~ 4 Gyr.